Title

Microbial community dynamics and coexistence in a sulfide-driven phototrophic bloom

Authors

Srijak Bhatnagar†, Elise S. Cowley†, Sebastian H. Kopf, Sherlynette Pérez Castro, Sean Kearney, Scott C. Dawson, Kurt Hanselmann, S. Emil Ruff *

† Denotes equal contribution

* Corresponding author

Author Affiliations

SB: Geomicrobiology Group, University of Calgary, Alberta, Canada; srijak.bhatnagar@ucalgary.ca

ESC: Medical Scientist Training Program, School of Medicine and Public Health, University of Wisconsin-Madison, Madison, WI, USA; ecowley@wisc.edu

SHK: Department of Geological Sciences, University of Colorado, Boulder, CO, USA; sebastian.kopf@colorado.edu

SPC: Ecosystems Center/Bay Paul Center, Marine Biological Laboratory, Woods Hole, MA, USA; sperezcastro@mbl.edu

SK: Department of Biological Engineering, Massachusetts Institute of Technology, Cambridge, MA, USA; skearney@mit.edu

SCD: Department of Microbiology and Molecular Genetics, University of California Davis, CA, USA; scdawson@ucdavis.edu

KH: Department of Earth Sciences, ETH-Z, Zürich, CH; kurt.hanselmann@erdw.ethz.ch

SER: Ecosystems Center/Bay Paul Center, Marine Biological Laboratory, Woods Hole, MA, USA; eruff@mbl.edu

Keywords

Microbial succession, Green sulfur bacteria, Prosthecochloris, microbial bloom, brackish coastal ecosystem, anoxygenic phototrophy, Microviridae, virus, CRISPR-Cas, resilience

Abstract

Phototrophic microbial mats commonly contain multiple phototrophic lineages that coexist based on their light, oxygen and nutrient preferences. Here we show that similar coexistence patterns and ecological niches can occur in suspended phototrophic blooms of an organic-rich estuary. The water column showed steep gradients of oxygen, pH, sulfate, sulfide, and salinity. The upper part of the bloom was dominated by aerobic phototrophic *Cyanobacteria*, the middle and lower parts were dominated by anoxygenic purple sulfur bacteria (*Chromatiales*) and green sulfur bacteria (*Chlorobiales*), respectively. We found multiple uncultured phototrophic lineages and present metagenome-assembled genomes of two uncultured organisms within the *Chlorobiales*. Apparently, those *Chlorobiales* populations were affected by *Microviridae* viruses. We suggest a sulfur cycle within the bloom in which elemental sulfur produced by phototrophs is reduced to sulfide by *Desulfuromonas sp*. These findings improve our understanding of the ecology and ecophysiology of phototrophic blooms and their impact on biogeochemical cycles.

Background

Estuarine and coastal water bodies are dynamic and ubiquitous ecosystems that are often characterized by the mixing of terrestrial freshwater and ocean saltwater. Brackish habitats can have striking physical and chemical characteristics that differ from both fresh and saltwater ecosystems [1,2]. Brackish ecosystems are very diverse and support large microbial and macrobial communities [1]. Estuaries also provide crucial ecosystem services, the most salient of which are trapping and filtering terrestrial runoffs and pollutants before they enter the oceans, coastal protection, erosion control and habitat-fishery linkages [3–6].

Estuaries harbor abundant and diverse microbial communities that form the basis of a complex food chain by fixing carbon dioxide through photosynthesis or chemosynthesis [7–9]. Additionally, carbon introduced to estuaries as organic matter from the oceans or land can be remineralized by heterotrophic microbial communities [10–12]. The decomposition of sulfur containing organic compounds through fermentation can lead to the production of sulfide in estuarine sediments [13]. Furthermore, sulfate brought into estuaries by ocean waters can be used by sulfate reducers, which reduce sulfate into elemental sulfur or sulfide [13,14]. Sulfate introduced by ocean water and sulfide released from the sediments form gradients in the water column that cause a chemocline in the brackish water column [15]. Additionally, estuaries and

coastal marshes often exhibit a halocline, i.e. a change in salinity, and the depletion of oxygen in the water column can create an oxycline [16,17]. Overlapping gradients, e.g. in salinity, light availability, as well as oxygen and sulfide concentration can create habitats and niches that favor certain microbial communities and conversely microbial communities can affect and respond to such gradients [18–20].

Gradients of light availability, oxygen and sulfur concentrations in stratified aquatic environments offer the development for complex and stable microbial assemblages [21]. These gradients are usually divided into a surface layer rich in oxygen, an intermediate layer with decreasing oxygen and a bottom anoxic layer. The surface layer is often dominated by oxygenic phototrophic microorganism such as *Cyanobacteria*. The anoxic layer, particularly in systems with high organic loads or seagrass beds, provides niches for anaerobes such as sulfate-reducing bacteria [22]. In the intermediate layer, anoxygenic phototrophs use the light from the surface and the sulfide from the bottom layers [23]. The biogeochemical processes leading to stratification in phototrophic blooms are relatively well understood [24], yet ecological niches, microbial interactions and community dynamics are less well constrained.

The abiotic and biotic drivers of stratified aquatic environments such as estuaries can fluctuate frequently and rapidly as a result of many factors, for example, tidal cycles, weather patterns, and seasonal cycles [25–30]. Such disturbances can bring about noticeable changes in the microbial community structure of the ecosystem. It was shown that estuarine communities were structured by salinity [31–34], precipitation [32,35], temperature [33,34], oxygen [35,36] and also seasonal changes [34]. These community shifts included changes in phytoplankton populations with salinity [31], declining populations of *Rhodobacterales* with decreasing salinity [35], declining populations of phototrophic *Ca.* Aquiluna with decreasing oxygen concentration, as well as general changes in the richness and evenness of the community [31–36].

Trunk River in Woods Hole, MA is a brackish ecosystem, on the coast of Vineyard Sound (N 41.535236, W -70.641298). Near the mouth, Trunk River forms a shallow lagoon where freshwater mixes with seawater. Storms, tides, and run-off introduce large amounts of biomass to the pond forming thick layers of decaying seagrass and other organic matter. The pond has a distinct sulfidic odor that emanates from the water and gases bubble up from the sediment. Bright yellow microbial blooms can be observed occasionally just below the water surface (see Figure 1, S1), forming and disappearing within days to weeks. Transient blooms were observed

to occur in natural depressions in the decaying organic matter and anecdotally seemed to be initiated by physical disturbance events, potentially from storms, tidal extremes, human activity, or animals. Given this visually striking natural ecological progression, we set out to test whether physical disturbance could trigger the blooms, and whether the established blooms could be used as a model system to investigate the microbial ecology and ecophysiology of sulfur-oxidizing phototrophs.

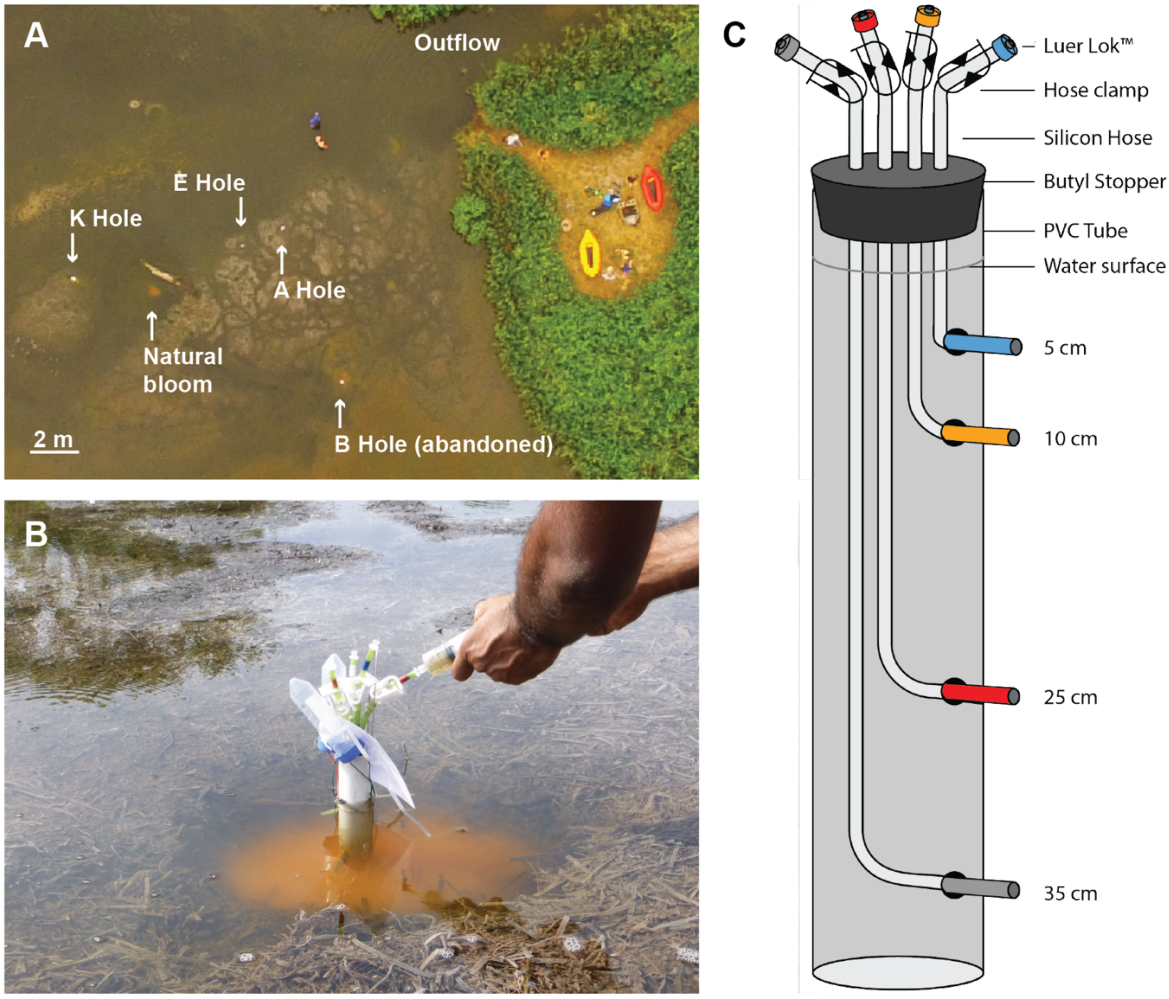

Figure 1: Sampling sites. A. Aerial view of experimental sites (A, E, and K) in the Trunk river lagoon. The water enters the lagoon from the right and exits to the sea through a channel marked outlet. **B.** View of a **LEMON** (**L**ong-term **E**nvironmental **MON**itoring) sampling device during sample collection on time point 3; 5 days post-disturbance. **C.** Schematic of the LEMON.

We mimicked physical disturbances of the brackish ecosystem by creating artificial depressions in the decaying organic matter, and monitored the microbial community response and population dynamics, as well as investigated ecological niches of the key populations. Based on the above described observations of thick layers of decaying organic matter and naturally occurring, rapid blooms of phototrophs, we hypothesized that i) the disturbance would release sulfide from the sediment and cause a sulfide-driven phototrophic bloom ii) due to its rapid development the bloom would likely be dominated by very few populations and iii) steep physicochemical gradients would establish that create (transient) anoxic habitats in the water column analogous to blooms in stratified lakes. We discuss the resulting reproducible ecological succession and provide insights into the habitats, niches and coexistence of phototrophic microorganisms. Our findings contribute to the understanding of the ecological processes and dynamics that shape phototrophic blooms, which are a naturally occurring phenomenon in many ecosystems.

Results

This study was designed to investigate microbial community assembly, community turnover and syntrophic interactions in a sulfide-driven phototrophic bloom. To gain insights into the microorganisms niches and potential key metabolisms we studied the physicochemistry of the water column and the diversity of photopigments, and performed amplicon and metagenomic sequencing.

Physicochemistry of the water column

At the first sampling time point (2 days post-disturbance), no difference in color was observed in the water column. Two days later, a faint pink layer was observed in the water column, and faint shades of yellow appeared in samples from the 25 cm depth (Figure S2, Supplementing Results). The yellow color of the suspension was most intense from timepoint 4 to 7 and had almost disappeared by timepoint 8. Within the first three days of the experiment the pH decreased between one and two units in all layers, with lowest values present in the deepest layer (Figure 2). Over the 15-day sampling period, pH showed more variation in the two upper layers than in the two deeper layers where it was very constant at values between 6 and 6.3. Throughout the experiment the water column in all three experiments showed a stable halocline with brackish water (5 ‰ salinity) at the water surface and saltwater (30 ‰) at 35 cm depth (Figure 2). Salinity increased with depth and was 12 ‰ and 23 ‰ at 10 cm and 25 cm, respectively. Major ions also

reflect this trend (e.g. calcium, potassium in Figure S6). The dissolved oxygen (DO) concentrations showed a relatively stable oxycline between 10 and 25 cm. At 10 cm and above, DO was mostly higher than 50 µM (91±45 µM) corresponding to ~20 % oxygen saturation (36±17 %). At 25 and 35 cm DO was mostly below 50 µM (23±18 µM), hence below ~20 % (9±9 %) saturation. The oxygen concentration slowly decreased in the upper two layers during the first half of the experiment but recovered again to the original values towards the end of the experiment. At 5 and 10 cm, DO averaged over the experiment was 101±47 µM and 81±41 µM , respectively (Figure 2). At 25 and 35 cm, the average DO was 28±22 µM and 17±11 µM, respectively. The sulfate concentrations in the water column decreased along the depth gradient, with the highest sulfate concentration at 5 cm (≈ 2 mM) and the lowest at 25 cm (≈ 0.2 mM) (Figure 2). In contrast, the sulfide concentrations were lowest at 5 cm (Figure 2F). Interestingly, the greatest sulfide concentration was measured at 10 cm depth peaking at over 1 mM towards the end of the experiment. Below 10 cm, sulfide concentration was still high, but declined to 0.75 mM ± 0.22 at 25 cm and 0.5 mM ± 0.17 at 35 cm. The normalized biomass measured for the 5 cm samples throughout the sampling period was nearly zero (Figure 2). At 10 cm, 25 cm, and 35 cm, the normalized biomass measured was approximately, 0.2 mg/mL, 0.3 mg/mL, and 0.2 mg/mL, respectively. For details concerning iron (Fe(II), Fe(III), total Fe), nitrate, calcium, potassium, ammonium and acetate refer to Supplementary Results and Figure S6. Overall, the measurements revealed stable and reproducible physicochemical gradients that divided the previously homogenous water column into layers with different redox conditions and energy availability.

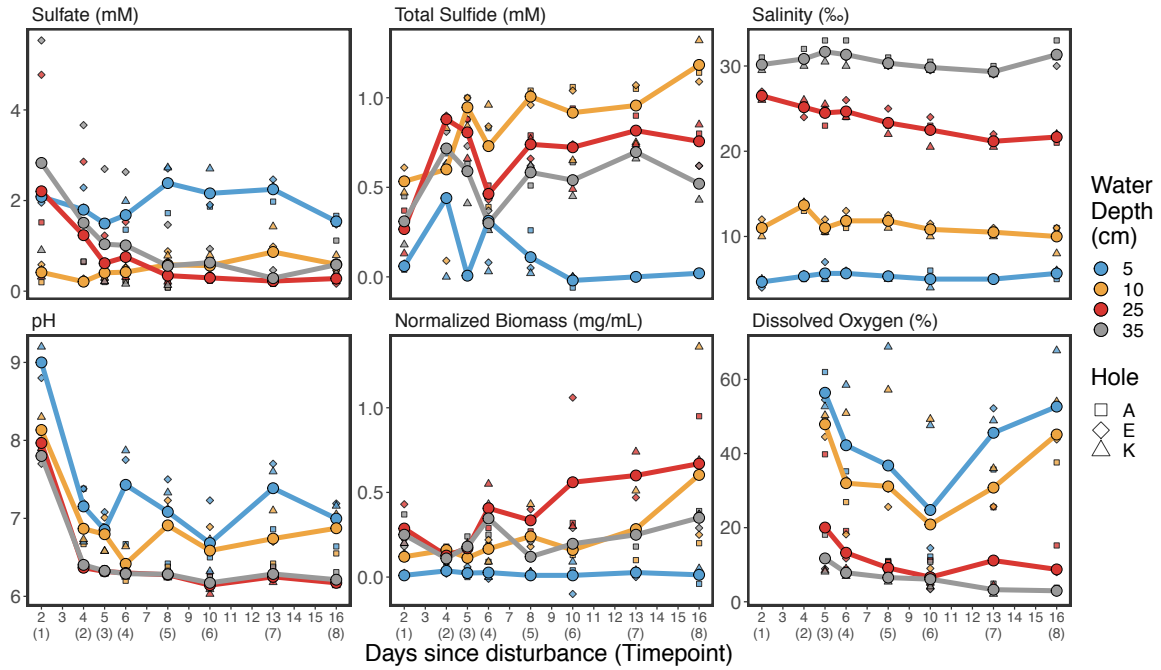

Figure 2: **Physicochemical measurements at the sampling sites**. Measurements are shown as averages (circles) across the three replicate holes. Measurements at individual holes are shown as squares, diamonds and triangles, the trend is shown as lines connecting average values. The x-axis shows days since disturbance and sampling timepoints in brackets. The y-axis shows the respective units. For an alternative representation of the physicochemical parameters as depth profiles instead of temporal profiles, see Figure S5. For further parameters (Fe (II); Fe (III); Total Fe, nitrate) refer to Figure S6.

Spectral Absorbance of Phototrophic Community

We measured absorbance spectra from filters of samples from A, E and K experiments (Figure 5A) and compared the spectra to those of representative cultured species of the most abundant phototrophic genera from the literature [37–41] (Figure 5B). Our results show that pigments belonging to PSB (purple vertical bands) were prominent in the upper layer of the bloom (orange spectra in 5A) especially between day 10 and 13, while GSB pigments (green vertical band in 5A) dominated the lower layers of the bloom (red and gray spectra) starting at day 10. Pigments characteristic for *Cyanobacteria* (brown vertical band) were less abundant in the bloom but increased at the end of the experiment relative to the PSB and GSB peaks. This suggests a minor role of *Cyanobacteria* initially and during the bloom but a more important role upon return to equilibrium. Pigments of all major phototrophs were detected throughout the experiment (gray vertical band). The spectral results suggest the coexistence of multiple phototrophic lineages over the entire duration of the experiment.

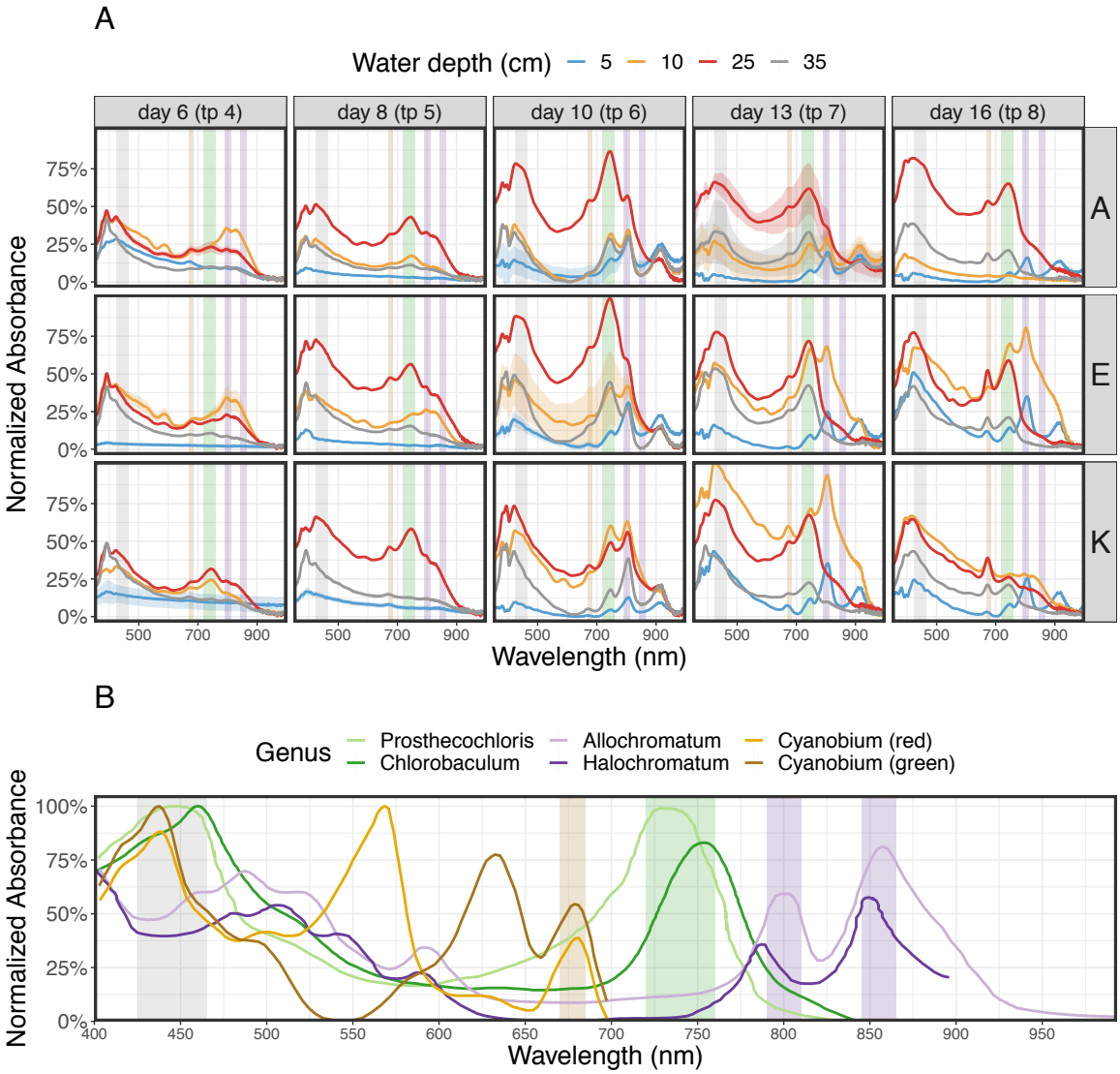

Figure 3: **Spectral Absorbance**. A) Sample spectra for the 3 sites at 5 different time points each showing averages of at least three replicate spectral analyses per sample. Significance bands along the spectra indicate one standard deviation (bands are mostly smaller than center line and thus not visible). Vertical bands indicate major absorbance peaks of the GSB group in green (*Prosthecochloris* and *Chlorobaculum*, 720-760 nm) and the PSB group purple (*Allochromatium* and *Halochromatium*, 790-810 nm and 845-865 nm) highlighting the transient appearance and likely dominance of these phototrophs over the course of the experiments. Also indicated is the general phototroph absorbance band in the 425-465 nm window in light gray. Cyanobacterial groups have distinct absorbance peaks in the 500-700 nm range that are not prominent in the sample spectra except for the characteristic 670-685 nm peak (light brown vertical band) reflecting the presence but likely smaller role of these taxa during the experiment. B) Absorbance spectra of pure culture representatives of major phototrophic groups with the same vertical bands as in panel A highlighting diagnostic absorbance peaks of GSB (in green), PSB (in purple), cyanos (in orange/brown) and phototrophs in general (in gray). All absorbance spectra were normalized to the respective highest peak.

192 Microbial Community Structure and Taxonomic Composition

193 At the beginning of the experiment, the microbial diversity was high in all four water depths and
194 very similar across replicate ecosystems. Alpha diversity rapidly decreased with the onset of the
195 bloom, and within two days the communities in the four depth layers substantially changed
196 (Figure 4, 5, S7, S8). The bloom occurred between 10 – 30 cm water depth (Figure S2) with
197 highest cell numbers (peaking at $>10^8$ cells ml^{-1}) and biomass at around 25 cm water depth
198 (Figure 2, S4) in brackish, mildly acidic, and hypoxic waters (Figure 2). The number of observed
199 amplicon sequence variants (ASV), as well as estimated richness, Shannon entropy, and Inverse
200 Simpson diversity significantly decreased between the surface water and the water at a depth of
201 10 cm and 25 cm (Figure 4; $p=0.001$). This change is most striking in the case of Inverse
202 Simpson diversity, a measure for evenness. In just one day, evenness dropped in both 10 cm and
203 25 cm water depth by over one order of magnitude to low single digit values (Figure 4; Table
204 S1). This means the community was dominated by one ASV (a pure culture has an Inverse
205 Simpson diversity index of 1). This decrease in diversity was accompanied by a substantial
206 decrease in pH, as well as an increase in sulfide concentration.

207 The rapid and profound change of community structure is corroborated by a high turnover of
208 ASV between the layers and timepoints (Figure 5, S8). The top layer is well separated from the
209 deeper layers. The communities at 25 cm water depth experienced the largest turnover, i.e.
210 change in community structure, and showed a loss in diversity during the experiment that
211 seemed to have recovered at the last time point (Figure 5). The communities of all three deep
212 layers (15 – 35 cm) had a similar community structure at the beginning of the experiment.
213 Interestingly, during the course of the experiment the community structure of each layer
214 followed a different trajectory, yet at the end converged again. The trajectories of layer 2-4
215 indicate that the bloom shifted the microbial communities in these layers to an alternative stable
216 state.

217

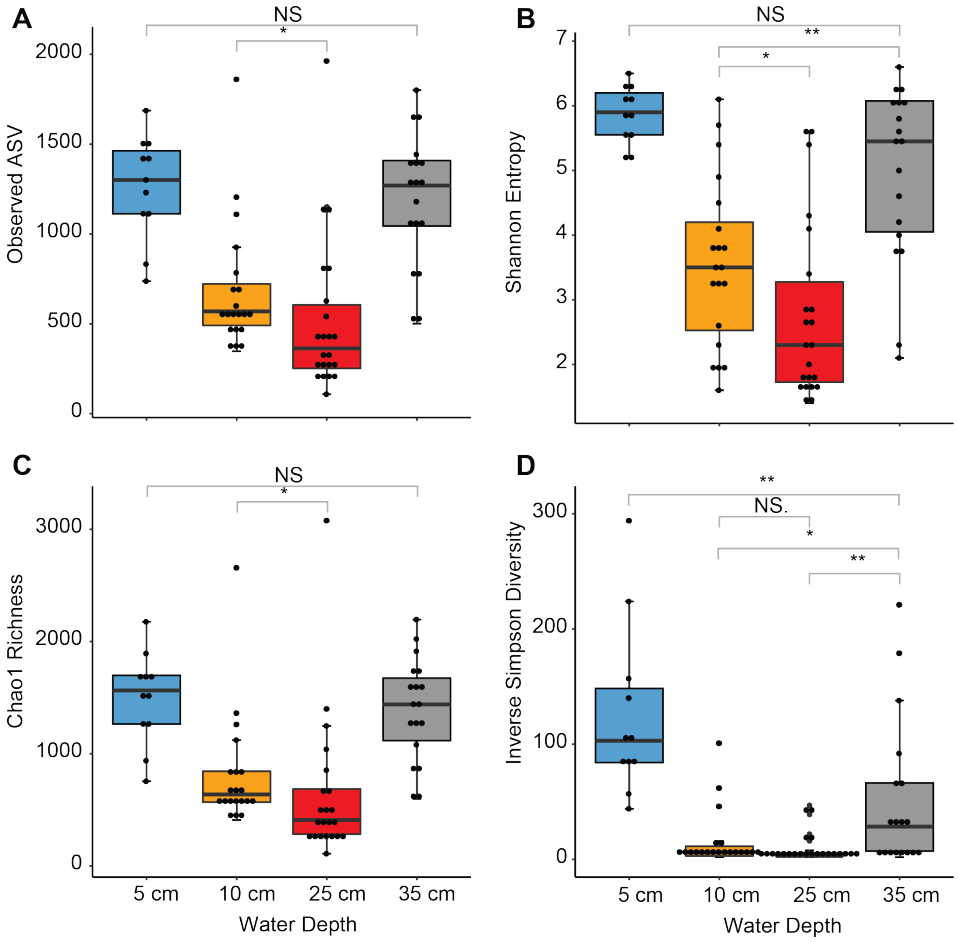

Figure 4: Diversity Indices of all samples shown as boxplots grouped by depth. Pairwise comparisons with low significance levels are shown (NS, *: p<0.1, **: p<0.01). All pairwise comparisons that are not shown were highly significant (***: p<0.001), e.g. panel A 5 cm vs 10 cm.

The taxonomic composition was assessed at all phylogenetic levels (Figure 6, S9). We observed a total of 73 bacterial phyla. The surface community (5 cm) remained relatively unchanged throughout the experiment and was dominated by *Proteobacteria*, *Chlorobi*, *Cyanobacteria* and *Actinobacteria*. The communities in the deeper oxygen poor and sulfide rich zones (10 – 35 cm) were more dynamic, being dominated by *Bacteroidetes*, *Proteobacteria*, *Firmicutes*, and *Chloroflexi*. In general, taxonomic diversity was highest in the deepest layer (35 cm). The profound change in diversity was accompanied by a change in composition. Within a few days, there was a substantial increase in the abundance of *Chlorobi*, which comprised more than 75% of the community at that time. This increase persisted for nine days, but levelled off at the end of the experiment. The datasets of all layers and timepoints were dominated by ASVs affiliating

with phototrophic organisms, as shown by relative sequence abundances on genus level (Figure 6A). Some phototrophs occurred in all layers at similar relative sequence abundances, such as *Halochromatium* and "*Candidatus* Chloroploca". The stable surface layer harbored *Cyanobium* and "*Candidatus* Aquiluna", which decreased in the deeper layers. The upper layer of the bloom showed an increased relative sequence abundance of *Allochromatium,* the lower bloom layer was dominated by *Prosthecochloris* and *Chlorobaculum* (Figure S11). In addition to phototrophs the bloom layers were enriched with sulfur-reducing *Desulfuromonas sp.* as well as *Exiguobacterium sp.* (Figure 6, Figure S9, S11). The layer above the bloom was slightly enriched with sulfur-oxidizing *Thiovirga sp.* and the layer below the bloom with *Erypsipelothrix sp.* Sulfate-reducing *Desulfobacteraceae* and *Desulfobulbaceae* were observed at low relative abundances in all layers (Figure S9B).

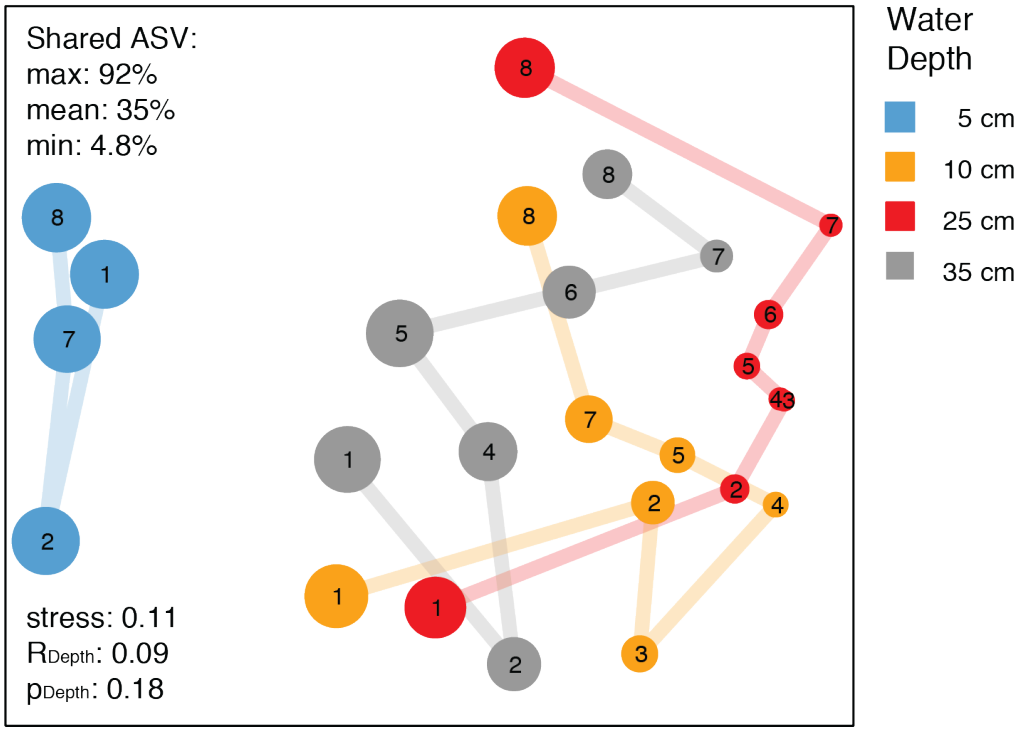

Figure 5: Microbial Community Turnover. Non-metric multidimensional scaling (NMDS) ordination based on relative abundance of ASV (amplicon sequence variants). Each circle represents one sample, the closer two samples are the more similar is their microbial community structure. Circle size represents Shannon Diversity. Numbers indicate sampling time points. Colors indicate bloom layers. Note: Individual holes were very similar (see Figure S8A) and thus we averaged relative ASV abundances for clarity, i.e. each circle represents an average across replicate experiments. NMDS ordinations for individual experiments are shown in Figure S7. The communities in the different layers of individual experiments are significantly different yet overlapping (see Figure S7).

254 Interestingly, almost all *Prosthecochloris* affiliated reads belonged to a single sequence variant,
255 while ASV diversity affiliated with the closely related *Chlorobaculum* increased over time
256 (Figure 6B, S10). The relative sequence abundance of *Chlorobiales* noticeably changed at 25 cm
257 depth, where the yellow microbial bloom was visually observed. *Chlorobiales* ASVs accounted
258 for >25 % of reads in our dataset. To identify the phylogeny of ASV affiliating with
259 *Chlorobiales*, we placed the representative sequence of each ASV on a reference tree of known
260 *Chlorobiales*. The most abundant *Chlorobiales* ASV (ASV_1) affiliated with the genus
261 *Prosthecochloris*, and specifically in the monophyletic clade of *Prosthecochloris vibrioformis*
262 (Figure S12), followed by an ASV (ASV_2) affiliating with *Chlorobaculum*. Together, these two
263 ASVs account for >97 % of the *Chlorobiales* reads. In general, we found a high number of
264 unclassified lineages. The 20 most abundant ASV accounted for about 50 % of all sequences,
265 twelve of those belonged to unclassified genera or families (Figure S9B). The novelty was
266 especially high within the *Chromatiaceae* five of the eight ASV that ranked among the "top 20"
267 belonged to an unclassified genus.

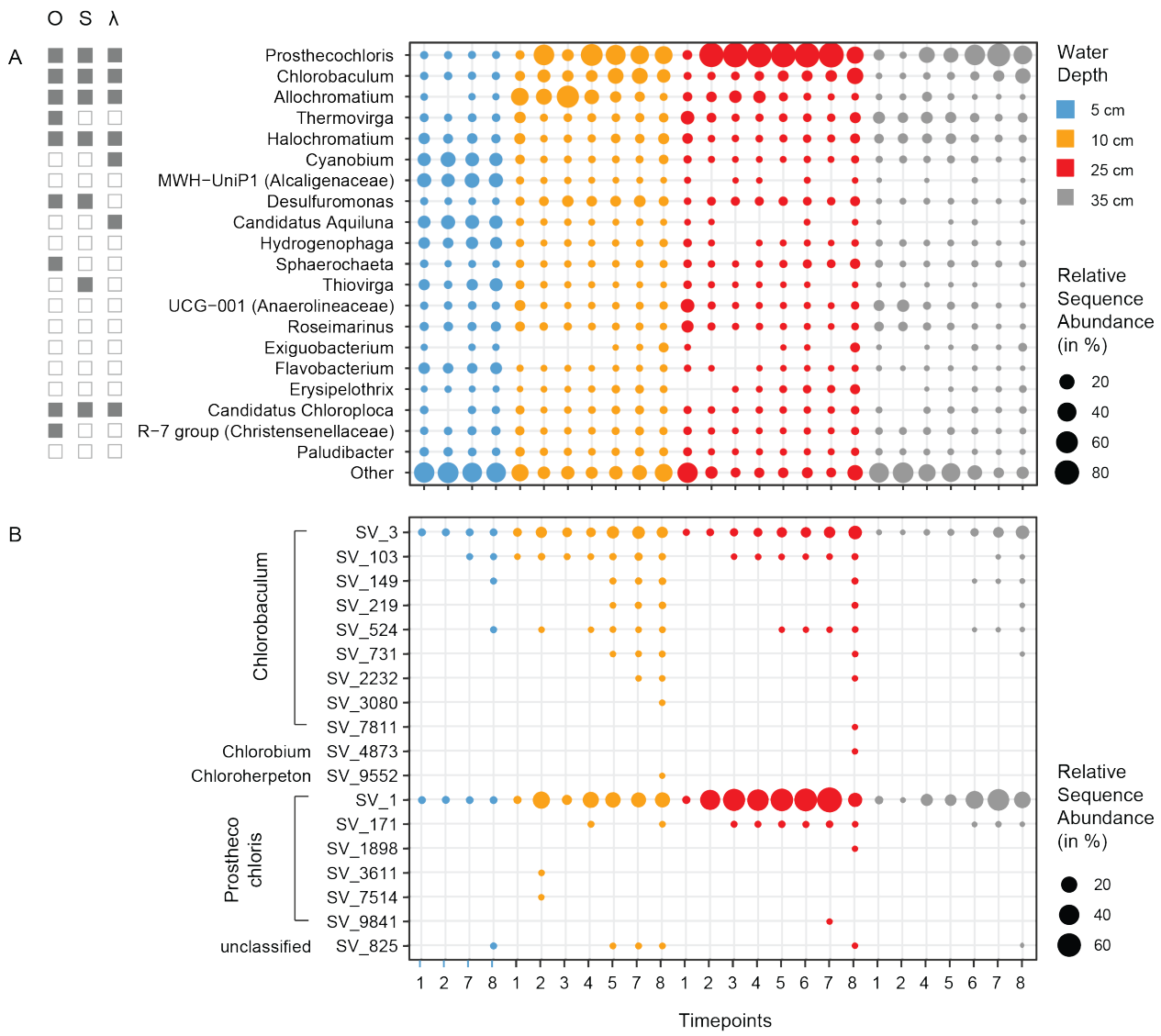

Figure 6: Microbial community composition on genus level. A: Relative sequence abundance of genera found in different depths (colors) and timepoints (x-axis). Relative sequence abundances were averaged across triplicates, due to the high similarity of all three experiments. Clades that are anaerobic (O), involved in the sulfur cycle (S), or phototrophic (λ) are indicated by full squares. B: Relative sequence abundance of amplicon sequence variants (ASV) within the order *Chlorobiales*. The graph shows average values of the three replicate experiments for clarity. The replicate experiments were very similar (see SI Figure S5 and S6).

Metagenomics-derived insights into *Chlorobiales* populations

We calculated the index of replication (iRep) [42] of the *Prosthecochloris* and *Chlorobaculum* populations based on the metagenome-assembled genomes (MAGs) that were recovered from the community metagenomes of two replicate experiments (Replicates A, E) and the enrichment

281 culture (SK) at timepoint 7. Both populations were replicating rapidly. *Prosthecochloris* (bin10)
282 had an iRep value of 3.7 (r^2=0.90, sample 7A3), which indicates that on average every cell had
283 2.5 replication events at the time of sampling. *Chlorobaculum* (bin 6) had iRep values of 2.5
284 (r^2=0.95, sample 7E3) and 2.8 (r^2=0.95, sample 7K3), indicating that on average every cell had
285 ~1.5 replication events. Both MAGs contained genes of the thiosulfate-oxidizing multienzyme
286 system (Sox). Bin 6 contained SoxXYZAB while Bin 10 contained only SoxYZ (Figure S17).
287 Both MAGs also contained the sulfate reductase subunit DsrAB involved in sulfate reduction,
288 and components of assimilatory sulfate reduction (CysND and Cys). Genes for
289 bacteriochlorophhyll (BChl) biosynthesis (bchEMU) were found in both MAGs. Bd-type
290 oxidases (CydAB) were present in both MAGS, while heme-copper oxygen reductases were
291 only found in Bin 6 including several cytochrome c oxidases (COX10, CyoABCDE and III)
292 (Table S4).

293 Bin 6 (*Chlorobaculum sp.*) and bin 10 (*Prosthecochloris sp.*) contain CRISPR arrays denoted as
294 either type I (cas3) or III (cas10) CRISPR systems [43] (Figure S18, S19). CRISPR predictions
295 revealed 3 direct repeat sequences in both MAGs of 30 and 35 (2) bp in length for Bin 6 and 37,
296 32, and 33 for the Bin 10 (Table S5). None of the spacers were shared by the closest reference
297 and representative genomes or matched sequences in the CRISPR database [44]. However, a
298 highly similar CRISPR array and direct repeat sequence were found between our Bin 6 and
299 *Chlorobaculum parvum* NCBI8327 with 60% *cas* genes similarity (Figure S18). The
300 metagenomes of all experiments, as well as of the GSB enrichment culture contained high
301 relative sequence abundances of viruses affiliating with *Microviridae* (Figure S20).

302

303 **Discussion**

304 In this study, we created artificial depressions in the decaying seagrass layer of Trunk River to
305 mimick disturbances that naturally occur at this site. We performed triplicate experiments that
306 showed very similar physicochemical gradients and patterns of community structure enabling us
307 to study microbial community succession in a natural setting. The observed slight variations
308 between replicate sites were likely due to differences in the organic matter composition and
309 distance to the lagoon access, or due to ripples and disturbances caused by weather, animals, and
310 sampling scientists. The replicated disturbances of the organic matter layers (A-hole, E-hole, and

311 K-hole) released trapped sulfide and caused the rapid establishment of steep physicochemical
312 gradients as well as the development of a bloom of sulfide-oxidizing phototrophs. We monitored
313 the microbial community assembly and succession, highlight the ecological niches of key
314 populations and indicate syntrophic interactions between phototrophs and sulfur reducers.

315 Sulfur cycling in the phototrophic bloom

316 Sulfate concentrations in the bottom layers decreased substantially within the first days and were
317 lowest in the bloom layer at 25 cm depth, where sulfate was almost entirely depleted. We found
318 sulfate-reducers affiliating with *Desulfobacteraceae* and *Desulfobulbaceae* in the hypoxic layers
319 of the bloom (Figure S9B) likely producing sulfide using either hydrogen or organic acids, e.g.
320 acetate (Figure S6) released from fermented organic matter. The sulfide concentrations were
321 highest at the upper boundary of the bloom at 10 cm water depth after the system stabilized
322 around day 6 (Figure 2). This is unexpected since reduced sulfur species, especially hydrogen
323 sulfide, are the electron donor for the green and purple phototrophs and thus should have been
324 depleted in these layers. At the same time, we found an increased relative abundance of sulfur-
325 reducing *Desulfuromonas sp.* in the bloom layers, peaking at around 15 % relative sequence
326 abundance. *Desulfuromonas sp.* are known to live in freshwater ecosystems and reduce
327 elemental sulfur to sulfide [45–47], which in turn can be reused by the sulfide-oxidizing
328 phototrophs. Our findings suggest that the initially present sulfide was released from the
329 sediment but was likely replenished by sulfate reducers from sulfate, as well as by sulfur
330 reducers from sulfur. Sulfide (and thiosulfate) are oxidized to elemental sulfur by the anoxygenic
331 phototrophs and hence the potential sulfur reduction by *Desulfuromonas sp.* indicates sulfur
332 cycling carried out by multiple species (Figure 7). A similar synergistic interaction was
333 suggested to occur in Lake Cadagno between sulfur disproportionating *Desulfocapsa*
334 *thiozymogenes* and purple sulfur bacteria affiliating with *Lamprocystis* [48]. At early timepoints
335 the microbial suspension was beige and milky, indicating the presence of large amounts of
336 elemental sulfur in the sample (Figure S2). Later the samples turned more yellow, due to an
337 increase in phototrophic organisms and their photopigments (Figure 2, 3), but also cleared up and
338 became translucent (Figure S2). Taken together these findings could mean that *Desulfuromonas*
339 *sp.* reduced the elemental sulfur (possibly present as polysulfides) that was produced by the
340 anoxygenic phototrophs before it accumulated in the suspension. An observation that merits
341 future research. Such a sulfur loop provides a positive feedback that could explain the

342 enrichment of sulfide in the bloom as well as the very rapid development of the sulfur-oxidizing
343 phototrophs. The involved *Chlorobi* and *Deltaproteobacteria* could even form tight aggregates
344 similar to *Chlorochromatium aggregatum* [49], to efficiently use the sulfur intermediate.

345 Assembly and coexistence of phototrophic microorganisms

346 The multispecies phototrophic bloom (fondly termed "microbial lemonade", Figure 1C) formed
347 around two to four days post-disturbance and was fully established by day six. The bloom
348 contained lineages from multiple phyla but was dominated by green and purple sulfur bacteria.
349 The color of the bloom slightly shifted from yellow-white at early timepoints to yellow-orange at
350 mid timepoints to yellow-green at late timepoints (Figure S2), likely due to the relative influence
351 of the photopigments of green and purple sulfur bacteria. The change in bacteriochlorophylls is
352 reflected by the pigment spectra collected at the different timepoints (Figure 3). The opacity and
353 color of the suspension, especially at the beginning of the experiment, is likely influenced by the
354 presence of polysulfides that are produced abiotically [50], as well as biotically by purple and
355 green sulfur bacteria due to their lack of the soxCD genes [51].

356 Interestingly, the sequencing data suggested that especially the lower layer of the bloom was
357 dominated by an apparently clonal population of green sulfur bacteria affiliated with
358 *Prosthecochloris vibrioformis*. The green sulfur bacteria are sulfur-oxidizing, strictly anaerobic,
359 obligate photoautotrophs [52]. Yet, based on our oxygen measurements, the Trunk River GSB
360 populations apparently tolerated relatively high oxygen concentrations of around 30 µM, but up
361 to 80 µM (Figure 2). The low concentration of dissolved oxygen at 25 cm depth combined with
362 sulfide, salinity, and low light created an optimal habitat for *Prosthecochloris sp*. The observed
363 community turnover (Figure 4) indicates that communities in the layers 2-4 shifted from one
364 stable state at the beginning of the experiment (timepoint 1) to an alternative stable state at the
365 end of the experiment (timepoint 8). It appears that PSB (*Allochromatium sp.*) played a key role
366 in stable state one, while the community of stable state two was equally dominated by both GSB
367 populations (*Prosthecochloris sp.* and *Chlorobium sp.*). The change of relative abundances of
368 phototrophs over the course of the experiment seems to be responsible for the pronounced
369 community turnover, because together these few clades made up the majority of sequence reads.
370 The high affinity for sulfide and the efficient growth of GSB at low light conditions [53] may
371 have enabled GSB to outcompete PSBs at the end of the experiment leading to a community
372 adapted to the changed conditions.

373 Despite the dominance of few populations the disturbance created a habitat with gradients of pH,
374 salinity, light, oxygen, and sulfide that enabled the coexistence of multiple phototrophic clades
375 from at least five different phyla (*Actinobacteria, Chlorobi, Chloroflexi, Cyanobacteria and*
376 *Gammaproteobacteria*). Coexistence of multiple phototrophic lineages was observed before,
377 especially in lakes [21,54,55]. The coexistence of organisms competing for the same energy
378 source is due to the different absorption maxima of each clades' photopigments (Figure 3), as
379 well as their need for different electron donors, and the varying salinity and oxygen tolerances of
380 each clade. At Trunk River *P. vibrioformis* is absent at 5 cm and present only in low abundance
381 at 10 cm. The surface layer (5 cm depth) is inhabited by oxygenic phototrophic *Cyanobacteria*
382 affiliating with *Cyanobium*, while the upper layer of the bloom (10 cm depth) is dominated by
383 purple sulfur bacteria of the order *Chromatiales* (Figure 6). Because *Prosthecochloris* are
384 adapted to low light conditions [56] and respond to different wavelengths of light than
385 *Cyanobacteria* and photosynthetic *Proteobacteria* [57,58], it is reasonable that they thrived at
386 depths of 25 cm, where they can out-compete other phototrophs. *Prosthecochloris* have been
387 previously observed in many marine and saline habitats, such as the Black Sea [59], Baltic Sea,
388 Sippewissett Salt Marsh, and Badwater basin [52]. They are considered to belong to a specialized
389 phylogenetic lineage of green sulfur bacteria adapted for marine and salt water ecosystems.
390 Blooms of *P. vibrioformis* have been previously observed in stratified lakes, where they
391 dominate the community at a specific depth [60], sometimes forming clonal blooms [61].

392 The suspended phototrophic bloom was spatially organized analogous to benthic phototrophic
393 mats in the nearby Sippewissett Salt Marsh [62–64] and elsewhere [65,66]. Thus, the disturbance
394 experiment that we performed *in situ* created a transient ecosystem with niches resembling those
395 in coastal microbial mats, except across a spatial scale that was one order of magnitude greater.
396 The community slowly collapsed after about two weeks and the water column seemed to return
397 to its original state (Figure 5). We did not observe a shift from phototrophic to chemotrophic
398 sulfur oxidation after the phototrophic bloom [21].

399 <u>New species of green sulfur bacteria and possible viral predation</u>

400 Due to the findings of a previous study based on 16S rRNA gene libraries, Imhoff and colleagues
401 proposed the existence of several uncultivated GSB species in Sippewissett Salt Marsh and other
402 estuaries [52]. The authors provide evidence that several GSB clades harbor species that have yet
403 escaped isolation, among those are species in the genera *Chlorobaculum* and *Prosthecochloris*.

404 We have strong evidence that we found at least two of these species based on our MAGs of a
405 *Chlorobaculum* species (Bin 6, Figure S13, S15) and a *Prosthecochloris* species (Bin 10, Figure
406 S13, S16). Both MAGs cluster sufficiently far away from the closest cultured isolate (Figure
407 S12, S14) and have average nucleotide identity (ANI) values of <90 to their respective closest
408 cultured isolate.

409 Physiological and functional characteristics cannot be easily deduced from the presence of genes
410 alone. Yet, it is very likely that the populations represented by bin 6 and 10 were sulfur
411 oxidizers, because their genomes encoded for enzymes performing thiosulfate oxidation. As in
412 most GSB, bin 6 contained the genes SoxABXYZ coding for enzymes that oxidize thiosulfate
413 to sulfate and polysulfides [67]. Bin 10 only contained SoxYZ (Figure S17). The absence of
414 SoxB genes has been identified in other non-thiosulfate oxidizing GSB such as the close relative
415 *Prosthecochloris estuarii*, or in *Chlorobium limicola* DSM 245 and *Chlorobium luteolum* DSM
416 273 [68]. Bacteriochlorophyll synthesis genes were identical in both Chlorobi MAGs coding for
417 pigments common to *Chlorobi*. In bin 6 we found complete operons encoding for cytochrome o
418 oxidase (CyoABCDE) and cytochrome d oxidase (CydAB) [69]. The latter was found also in bin
419 10, indicating that both organisms have means to cope with oxygen stress, hence explaining their
420 presence at relatively high oxygen concentrations and their ability of performing anoxygenic
421 photosynthesis under (hyp)oxic conditions.

422 Both MAGs also contain CRISPR-Cas systems that are very different from the cultured isolates
423 (Figure S18, S19). Our CRISPR results show that Trunk River populations may be under
424 predatory stress, affecting the abundance of bacterial blooms, and that host immunity is active in
425 this ecosystem [70]. The unique CRISPR arrays indicate that closely related species may be
426 infected by different viruses with species specificity [71]. However, some viral populations have
427 been reported to have broad host ranges [72]. Divergent evolution or strain level microdiversity
428 may also explain distinct CRISPR-Cas systems [73]. A lack of public databases containing viral
429 sequences restricts the detection of viral-host interactions [74]. While Llorens-Marès *et al.*
430 (2017) characterized a potential green sulfur bacterial viral infection, to date, phages infecting
431 *Chlorobi* have not been reported. Our analyses suggest that viruses of the family *Microviridae*
432 played a major role in the transient bloom (Figure S19), possibly even for its demise. This
433 interesting finding merits future research on transient phototrophic blooms in estuarine
434 ecosystems.

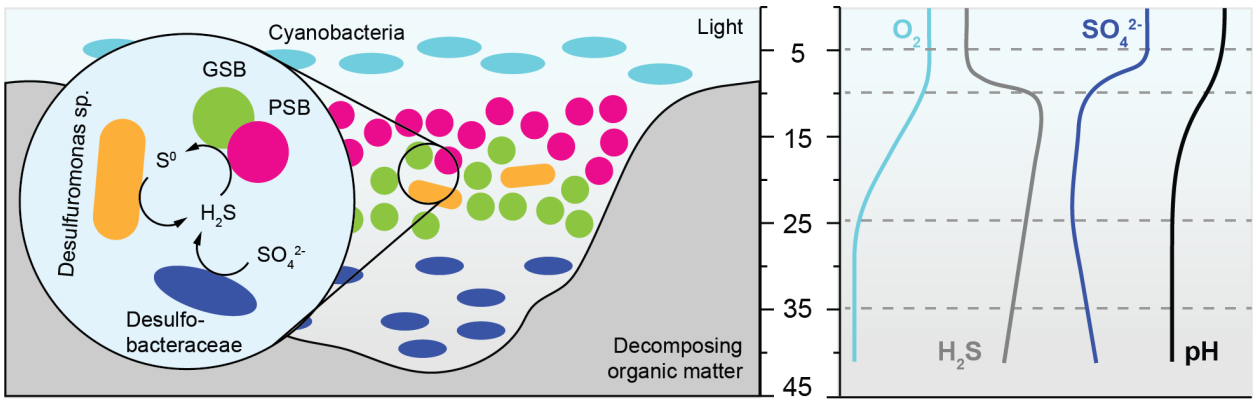

Figure 7: Schematic overview of the phototrophic bloom showing the main phototrophic populations, sulfur compounds, and chemical gradients.

Conclusions

In this study, we investigated phototrophic blooms that naturally occur in a brackish estuarine ecosystem to understand the underlying microbial and biogeochemical dynamics. We show that phototrophs belonging to different phyla spatially organized within the water column based upon their light and oxygen requirements forming a layered bloom, analogous to the layered communities in phototrophic microbial mats (Figure 7). The community composition of the bloom indicates the presence of a sulfur cycle between anoxygenic phototrophs and sulfur reducers that could explain the rapid development of the bloom. We identified metagenome assembled genomes of two novel species of green sulfur bacteria, belonging to *Chlorobaculum* and *Prosthecochloris*. The MAGs contained terminal oxidases that may allow the organisms to thrive in a hypoxic environment, as well as repeats that evidence of host-virus dynamics. The metagenome contained viral sequences suggesting that *Microviridae* viruses infect species within the *Chlorobiales*. Overall, Trunk River is an excellent model ecosystem to study the microbial ecology and ecophysiology of phototrophic blooms in a natural setting.

457 **Methods**

458 Experimental Setup and Sample Collection

459 We used custom-made sampling poles for long-term environmental monitoring of the water
460 column without disturbing the established gradients (LEMON; Figure 1B, C). The sampling
461 poles were placed in three replicate depressions (A-hole, E-hole, and K-hole) that we dug into
462 the thick layers of decaying organic matter (Figure 1A). In each of sites, a sampling pole was
463 placed such that the inlets sampled water at 5 cm, 10 cm, 25 cm, and 35 cm depth below the
464 surface (Figure 1B, C). Sampling poles were set up one day after the holes were dug out and
465 sampling began one day after set up (two days post disturbance), to allow disturbed sediment to
466 settle. Samples were collected over a 15-day period during July-August 2015. For each sample,
467 the first 5 ml were discarded, followed by collection of 100 ml of water in several sterile tubes
468 for further analyses. The tubes were transported on ice to the laboratory and stored at 4˚C. All
469 sample collections were carried out between 4 pm and 6 pm.

470 Enrichment cultures

471 To enrich for GSB we used a defined saltwater medium (400g/l NaCl, 60g/l $MgCl_2$*$6H_2O$, 3g/l
472 CaC_{l2}*$2H_2O$, 10g/l KCl) buffered at pH 7.2 with 5 mM MOPS. The medium contained 5 mM
473 NH_4Cl as N source, 1mM K phosphate (pH 7.2) as P source, 70 mM $NaHCO_3$ as C source, 10
474 mM $Na_2S_2O_3$ as electron donor, 1 mM Na_2S as reductant or electron donor, a multivitamin
475 solution prepared at 1000× in 10 mM MOPS at pH 7.2, and a trace metal solution prepared at
476 1000× in 20 mM HCl. Saltwater base, MOPS, N- and P-source, and trace metals were autoclaved
477 together in a Widdel sparging flask, cooled under a stream of N_2/CO_2 (80%:20%) gas. C-source,
478 electron donors and vitamins were added from filter-sterilized stock solutions after cooling. The
479 medium was inoculated with biomass removed from *in situ* enrichments of GSB grown on glass
480 slides using a 770 nm monochromatic LED. After inoculation, the bottle was kept in dark for 2-4
481 hours and then placed 5 cm away from a LED light source with the same specifications. After a
482 visible sign of growth – green coloration – the culture was filtered through 0.2 µm filter and used
483 for DNA extraction, similar to other samples.

484 Physicochemical Measurements

485 *In-situ* measurements of pH, temperature, dissolved oxygen, oxidation reduction potential
486 (ORP), and ion selective electrode (ISE) were carried out with a multi-parameter probe equipped

487 with a quarto probe (YSI Professional Series Model Pro). The probe was calibrated for pH with
488 4, 7, and 10 buffers and for dissolved oxygen using oxygen-saturated water and an anoxic
489 solution of sodium ascorbate and sodium hydroxide. After each sample collection the probe was
490 lowered into the water to each depth per site and after probe readings stabilized, the parameters
491 were recorded.

492 To measure biomass and pigment spectra, up to 10 ml of the collected sample was filtered
493 through a sterile Millipore filter (0.2 µm GTTP, 0.2 µm GNWP, or 0.22 µm GV). Filtrates were
494 washed twice with ammonium acetate solutions with the same ionic strength as each depth. The
495 filters were placed on aluminium foil, dried at 60°C overnight and subsequently weighed (Figure
496 S3). A Spectral Evolution SR1900 spectrophotometer was used to measure the spectrum of the
497 dried biomass on each filter with a scanning range of 350-1900 nm. The light source was a
498 Dyonics 60 W lamp.

499 After sterile filtration, the filtrate was used to measure anion, cation, and organic acid
500 concentrations using an ion chromatographer. The ion concentrations of samples were measured
501 by diluting filtrate 1:10 with Millipore water to a total volume of 2 ml. The diluted samples were
502 measured in triplicate using a ThermoFisher/Dionex ICS2100 equipped with an AS18 column
503 using a 13 minute, 33 mM NaOH isocratic program to measure anions and a CS12A column
504 using a 13 minute, 25 mM methane sulfonic acid isocratic program to measure cations. Samples
505 for organic acid analysis were filtered through 0.2 µm filters and 900 µL of filtrate was added to
506 100 uL of 5 M H_2SO4 to precipitate any compounds that might do so on the column. The
507 samples were centrifuged and the upper portion was removed for HPLC analysis. Samples were
508 analyzed on a BioRad Aminex HPX-87H column in isocratic elution mode with 5 mM sulfuric
509 acid.

510 Iron concentration was quantified using the ferrozine assay [75]. 4.5 ml filtrate were added on
511 site to 0.5 ml of 1 M HCl to prevent oxidation of any available Fe(III). For Fe(II), 50 µl filtrate
512 was added to 50 µl of 1M HCl and 100 µl of ferrozine (0.1% [wt/vol] in 50% ammonium
513 acetate) was added. For total iron, 50 µl filtrate was added to 50 µl of 10% hydroxylamine
514 hydrochloride in 1M HCl to reduce Fe(III) to Fe(II). Samples were added to 100 µl of ferrozine.
515 All samples were incubated for 15 min and a filtrates Absorbances were read in triplicate at 560
516 nm using a Promega plate reader. Ferrous ammonium sulfate was used as standard.

517 Sulfide concentrations were quantified using the Cline assay [76]. 1.5 ml filtrate were added on
518 site to 500 µl of zinc acetate solution (91 mM) to prevent oxidation of the sulfide. Cline reagent
519 (N, N-dimethyl-p-phenylenediamine sulfate, H_2SO_4, $NH_4Fe(SO_4)_2 \cdot 12\ H2O$) was added, the
520 samples were incubated in the dark for 30 minutes and absorbance was read at 665 nm. A table
521 with all physicochemical and biomass measurements is publicly available at PANGAEA
522 (https://doi.pangaea.de/10.1594/PANGAEA.900343)

523 DNA Extraction, Library Preparations, and Sequencing

524 Within 2 – 6 hours of sample collection, 50 ml sample was filtered using an autoclaved 0.2 µm
525 polycarbonate filter (GTTP Millipore) and stored at -20˚C. Each filter was cut with a sterile
526 blade and extracted with the MoBio PowerFecal kit. We followed the protocol, but instead of
527 bead beating, the samples were twice vortexed horizontally with the beads (10 min and 20 min
528 with a 10 min pause). DNA concentration and purity were measured with Nanodrop and
529 Promega Qubit fluorometer and Nanodrop, respectively.

530 We prepared 16S rRNA gene amplicon library using V4-V5 fusion primers as previously
531 described [77]. Briefly, the fusion primer contains TruSeq adapter sequences, barcodes, and the
532 forward or reverse 16S rRNA gene primers. The forward and reverse 16S rRNA gene primers
533 were 518F (CCAGCAGCYGCGGTAAN) and 926R (CCGTCAATTCNTTTRAGT). The PCR
534 conditions were as follows: initial denaturation of 94˚C for 3 min, 30 cycles of denaturation at
535 94˚C for 30 s, annealing at 57˚C for 45 s, extension at 72˚C for 1 min, and final extension at
536 72˚C for 2 min. The libraries were cleaned using Agencourt Ampure XP beads, quantified using
537 picogreen, pooled in equimolar ratios, and cleaned again using Agencourt Ampure XP beads a
538 second time. The indexed libraries were then sequenced on the Illumina MiSeq PE250 platform.

539 The DNA from the depth of 25 cm from timepoint 7 from the three replicates, as well as from a
540 phototrophic enrichment were used to generate whole-genome shotgun metagenomic library.
541 The DNA was sheared using Covaris sonicator, size selected for 500-600bp using Pippin prep,
542 and cleaned using Agencourt Ampure XP clean beads. The cleaned DNA was analyzed using
543 Bioanalyzer DNA1000 chip and used to prepare metagenomic library using Nugen Ovation
544 ultralow DR multiplex kit with manufacture supplied protocol. The libraries were then
545 sequenced on Illumina MiSeq PE250 platform. All the sequencing was performed at the Keck
546 facility at the J. Bay Paul Center at the Marine Biological Laboratory, Woods Hole, MA.

547 Amplicon Sequence Data Analyses

548 The amplicon data was demultiplexed in mothur v1.39.5 [78], followed by the trimming of 16S
549 rRNA gene amplification primers using Cutadapt v1.16 [79] with default parameters. The
550 primer-trimmed amplicon sequencing data was quality checked using DADA2 v1.9.0 R Package
551 [80]. In DADA2, the reads were trimmed at the first instance of quality drop below 8, an
552 expected error rate of 2, followed by trimming to 220bp and 200bp for forward and reverse
553 reads. Any reads that matched PhiX or had an ambiguous base were removed. An error profile
554 for the forward and reverse reads was generated using learnErrors function and then used to
555 merge the forward and reverse reads using the mergePairs function. The merged reads were used
556 to generate the amplicon sequence variants using makeSequenceTable function, which was then
557 filtered for chimeras using removeBimeraDenovo function. The amplicon sequence variants
558 were assigned taxonomy in DADA2 using Silva reference database v132 [81]. Community
559 analyses were performed using a custom workflow based on R and the packages vegan, labdsv,
560 tidyverse (stringr, dplyr, ggplot2), UpSetR and custom scripts [82–87] for details see. Relative
561 abundance of bacterial ASV (amplicon sequence variants), Bray-Curtis dissimilarities,
562 Nonmetric Multidimensional Scaling as well as analyses determining Singletons and percent
563 shared ASVs are based on the unaltered Sample×ASV table as calculated by DADA2. The
564 ASV×Sample table including taxonomy is available at PANGAEA
565 (https://doi.pangaea.de/10.1594/PANGAEA.900354). To compare the diversity between samples
566 using the number of observed species, Shannon index, Inverse Simpson diversity and Chao1
567 Richness [88] the ASV abundance tables were rarefied to account for unequal sampling effort
568 using 31,682 randomly chosen sequences without replacement. For details refer to the R
569 workflow available at the public database PANGAEA
570 (https://doi.pangaea.de/10.1594/PANGAEA.900344).
571

572 Metagenomic Sequence Data Analyses

573 Quality control of the raw reads was performed using Preprocessing and Information of
574 SEQuence data (PRINSEQ) to remove sequencing tags and sequences with mean quality score
575 lower than 25, duplicates and N's [89]. All runs combined provided a total of approximately 3.5
576 million 250 bp read pairs. All forward and reverse reads were placed together in one file and
577 cross co-assembled using SPAdes using the --meta option [90]. Binning was performed using

578 MetaBAT [91] and Anvi'o (v5.2) metagenomic workflow (CONCOCT) [92]. Completeness and
579 contamination of bins was assessed using CheckM [93]. Assembled genomes that contained
580 more than 90% genome completeness, less than 5% contamination, and sequences mainly from a
581 single genus were further analyzed. This yielded two high quality bacterial metagenome-
582 assembled genomes (MAGs): Bin 6 and Bin 10. Taxonomic composition for each bin was
583 predicted using FOCUS [94]. Phylogenetic analysis including the identification of their closest
584 phylogenetic neighbors was investigated using PATRIC Comprehensive Genome Analysis [95].
585 Gene prediction for MAGs was performed using prodigal (V2.60, -p meta). We searched for
586 sulfur, terminal oxidases and chlorophyll pathways using Ghost-KOALA against the KEGG
587 GENES database. The *Chlorobi* bins 6 and 10 contained 2008 and 1938 predicted proteins,
588 respectively. CRISPRCasFinder [96] and CRISPRone [97] were used to identify CRISPR repeat
589 and spacer sequences. The quality checked reads from each sample were mapped to the MAGs,
590 Bin 6 and Bin 10 using bowtie2 [98]. The mapped reads were then analyzed using iRep [42] to
591 estimate replication events in Bin 6 and Bin 10. Unassembled sequences were processed on the
592 MG-RAST platform version 4.0.3. Percent abundance of viral sequences was calculated from the
593 RefSeq database using an e-value cutoff of 1e-5, a minimum identity cutoff of 60%, and an
594 alignment length minimum cutoff of 15 [99]. For details refer to the metagenome analyses
595 workflow publicly accessible at HackMD (https://hackmd.io/tGZyCM9sSNmuorpHenQVNA).

596 **Declarations**

597 Availability of data and material

598 The genomic datasets generated and analyzed during the current study are available on MG-
599 RAST (Project Name: Trunk River, ID: 4837589.3 (sample SK), 4837590.3 (sample 7K3),
600 4837591.3 (sample 7E3), 4837592.3 (sample 7A3)) and metagenome-assembled genomes
601 workflow are available on HackMD (https://hackmd.io/tGZyCM9sSNmuorpHenQVNA). The
602 raw 16S rRNA amplicon data, the shotgun metagenomic data, the 16S rRNA gene clonal
603 sequences, and the metagenome assembled genomes presented in this work are publicly archived
604 in NCBI under Bioproject PRJNA530984 (https://www.ncbi.nlm.nih.gov/bioproject/530984).
605 The contextual datasets generated and analyzed during the current study are publicly available at
606 PANGAEA under: https://doi.org/10.1594/PANGAEA.900343

607

608 Competing interests

609 The authors declare that they have no competing interests.

610 Funding

611 This work was carried out at the Microbial Diversity summer course at the Marine Biological
612 Laboratory in Woods Hole, MA. The course was supported by grants from National Aeronautics
613 and Space Administration, the US Department of Energy, the Simons Foundation, the Beckman
614 Foundation, and the Agouron Institute.

615

616 Authors' contributions

617 SB helped design the study, collected samples, prepared and analyzed sequencing data, wrote
618 manuscript

619 ESC helped design the study, collected samples, prepared and analyzed physicochemical data,
620 wrote manuscript

621 SHK helped design the study and enrichment cultures, analyzed physicochemical data and
622 pigment spectra, wrote manuscript

623 SPC analyzed metagenomic data, wrote manuscript

624 SK obtained enrichment culture, wrote manuscript

625 SD helped design the study, wrote manuscript

626 KH collected samples, prepared and analyzed physicochemical data and pigment spectra, wrote
627 manuscript

628 SER designed the study, analyzed and visualized sequencing and physicochemical data, wrote
629 manuscript with input from all co-authors

630 All authors read and approved the final manuscript.

631

632 Acknowledgements

633 We would like to express our deepest gratitude towards Dianne Newman and Jared R.
634 Leadbetter, directors of the Microbial Diversity Summer Course at the Marine Biological
635 Laboratory 2014-2017. Without their trust, support and encouragement the project would not
636 have been realized. We are very grateful to Joseph Vinneis, Kim Finnegan, and Mitchell Sogin
637 for providing laboratory space, equipment, and guidance regarding next-generation sequencing.
638 We are also very grateful to the students and staff of the 2015 Microbial Diversity Summer
639 Course, specifically Kurt Dahlstrom, Kristina Garcia, Jessica Choi, Rachel Soble, and Lina Bird.
640 We would like to thank the Simons Foundation, NSF, DOE, and NASA for funding the
641 Microbial Diversity Summer course, as well as Promega, Thermo Fisher Scientific, Spectral
642 Evolution, and MBL's Marine Resources Center for providing reagents and equipment used in
643 this work.

644

645 **References**

646 1. McLusky DS, Elliott M. The estuarine ecosystem: ecology, threats and management
647 [Internet]. Oxford University Press on Demand; 2004. Available from:
648 http://www.oxfordscholarship.com/view/10.1093/acprof:oso/9780198525080.001.0001/acprof-
649 9780198525080

650 2. Moore WS. The subterranean estuary: a reaction zone of ground water and sea water. Mar
651 Chem [Internet]. 1999;65:111–25. Available from:
652 http://www.sciencedirect.com/science/article/pii/S0304420399000146

653 3. Pant HK, Reddy KR. Phosphorus Sorption Characteristics of Estuarine Sediments under
654 Different Redox Conditions. J Environ Qual [Internet]. American Society of Agronomy, Crop
655 Science Society of America, Soil Science Society; 2001 [cited 2019 Feb 13];30:1474. Available
656 from: https://www.agronomy.org/publications/jeq/abstracts/30/4/1474

657 4. Jay DA, Orton PM, Chisholm T, Wilson DJ, Fain AM V. Particle trapping in stratified
658 estuaries: Application to observations. Estuaries and Coasts [Internet]. Springer-Verlag; 2007
659 [cited 2019 Feb 13];30:1106–25. Available from: http://link.springer.com/10.1007/BF02841400

660 5. Nelson JL, Zavaleta ES. Salt Marsh as a Coastal Filter for the Oceans: Changes in Function
661 with Experimental Increases in Nitrogen Loading and Sea-Level Rise. PLoS One [Internet].
662 2012;7:e38558. Available from: https://doi.org/10.1371/journal.pone.0038558

663 6. Barbier EB, Hacker SD, Kennedy C, Koch EW, Stier AC, Silliman BR. The value of estuarine
664 and coastal ecosystem services. Ecol Monogr [Internet]. John Wiley & Sons, Ltd; 2011 [cited
665 2019 Jul 11];81:169–93. Available from: http://doi.wiley.com/10.1890/10-1510.1

666 7. Waidner LA, Kirchman DL. Aerobic anoxygenic photosynthesis genes and operons in
667 uncultured bacteria in the Delaware River. Environ Microbiol. 2005;7:1896–908.

668 8. Ritchie AE, Johnson ZI. Abundance and Genetic Diversity of Aerobic Anoxygenic
669 Phototrophic Bacteria of Coastal Regions of the Pacific Ocean. Appl Environ Microbiol
670 [Internet]. 2012;78:2858–66. Available from: http://aem.asm.org/content/78/8/2858.abstract

671 9. Boschker HTS, Vasquez-Cardenas D, Bolhuis H, Moerdijk-Poortvliet TWC, Moodley L.
672 Chemoautotrophic Carbon Fixation Rates and Active Bacterial Communities in Intertidal Marine
673 Sediments. PLoS One [Internet]. 2014;9:e101443. Available from:
674 http://www.ncbi.nlm.nih.gov/pmc/articles/PMC4086895/

675 10. Peduzzi P, Herndl GJ. Decomposition and significance of seagrass leaf litter (Cymodocea
676 nodosa) for the microbial food web in coastal waters (Gulf of Trieste, Northern Adriatic Sea).
677 Mar Ecol Prog Ser [Internet]. 1991;71:163–74. Available from:
678 http://www.jstor.org/stable/24817387

679 11. Smith S V, Hollibaugh JT. Coastal metabolism and the oceanic organic carbon balance. Rev
680 Geophys [Internet]. 1993;31:75–89. Available from: http://dx.doi.org/10.1029/92RG02584

681 12. Moran MA, Sheldon WM, Zepp RG. Carbon loss and optical property changes during long-
682 term photochemical and biological degradation of estuarine dissolved organic matter. Limnol
683 Oceanogr [Internet]. 2000;45:1254–64. Available from:
684 http://dx.doi.org/10.4319/lo.2000.45.6.1254

685 13. Capone DG, Kiene RP. Comparison of microbial dynamics in marine and freshwater
686 sediments: contrasts in anaerobic carbon catabolism. Limnol Oceanogr. 1988;33:725–49.

687 14. Purdy KJ, Embley TM, Nedwell DB. The distribution and activity of sulphate reducing
688 bacteria in estuarine and coastal marine sediments. Antonie Van Leeuwenhoek [Internet].
689 2002;81:181–7. Available from: https://doi.org/10.1023/A:1020550215012

690 15. Zopfi J, Ferdelman TG, Jørgensen BB, Teske A, Thamdrup B. Influence of water column
691 dynamics on sulfide oxidation and other major biogeochemical processes in the chemocline of
692 Mariager Fjord (Denmark). Mar Chem [Internet]. 2001;74:29–51. Available from:
693 http://www.sciencedirect.com/science/article/pii/S0304420300000918

694 16. Long RR. Mass and salt transfers and halocline depths in an estuary. Tellus [Internet].
695 1976;28:460–72. Available from: http://dx.doi.org/10.1111/j.2153-3490.1976.tb00695.x

696 17. Lee DY, Owens MS, Doherty M, Eggleston EM, Hewson I, Crump BC, et al. The Effects of
697 Oxygen Transition on Community Respiration and Potential Chemoautotrophic Production in a
698 Seasonally Stratified Anoxic Estuary. Estuaries and Coasts [Internet]. Springer US; 2015 [cited
699 2019 Feb 13];38:104–17. Available from: http://link.springer.com/10.1007/s12237-014-9803-8

700 18. Wimpenny JWT, Wiegel J, Kuenen JG. Responses of Microorganisms to Physical and
701 Chemical Gradients [and Discussion]. Philos Trans R Soc Lond B Biol Sci [Internet].
702 1982;297:497–515. Available from: http://www.jstor.org/stable/2395933

703 19. Jørgensen BB, Revsbech NP. Colorless Sulfur Bacteria, Beggiatoa spp. and Thiovulum spp.,
704 in O2 and H2S Microgradients. Appl Environ Microbiol [Internet]. 1983;45:1261–70. Available

from: http://aem.asm.org/content/45/4/1261.abstract

20. Møller MM, Nielsen LP, Jørgensen BB. Oxygen Responses and Mat Formation by Beggiatoa spp. Appl Environ Microbiol [Internet]. 1985;50:373–82. Available from: http://aem.asm.org/content/50/2/373.abstract

21. Pjevac P, Korlević M, Berg JS, Bura-Nakić E, Ciglenečki I, Amann R, et al. Community shift from phototrophic to chemotrophic sulfide oxidation following anoxic holomixis in a stratified seawater lake. Appl Environ Microbiol [Internet]. American Society for Microbiology; 2015 [cited 2019 Mar 28];81:298–308. Available from: http://www.ncbi.nlm.nih.gov/pubmed/25344237

22. Wasmund K, Mußmann M, Loy A. The life sulfuric: microbial ecology of sulfur cycling in marine sediments. Environ Microbiol Rep [Internet]. John Wiley & Sons, Ltd (10.1111); 2017 [cited 2019 Jul 23];9:323–44. Available from: http://doi.wiley.com/10.1111/1758-2229.12538

23. Bush T, Diao M, Allen RJ, Sinnige R, Muyzer G, Huisman J. Oxic-anoxic regime shifts mediated by feedbacks between biogeochemical processes and microbial community dynamics. Nat Commun [Internet]. Nature Publishing Group; 2017 [cited 2019 Jul 23];8:789. Available from: http://www.nature.com/articles/s41467-017-00912-x

24. Zhu K, Lauro FM, Su H. Stratification Modelling of Key Bacterial Taxa Driven by Metabolic Dynamics in Meromictic Lakes. Sci Rep [Internet]. Nature Publishing Group; 2018 [cited 2019 Jul 23];8:9538. Available from: http://www.nature.com/articles/s41598-018-27973-2

25. Haas LW. The effect of the spring-neap tidal cycle on the vertical salinity structure of the James, York and Rappahannock Rivers, Virginia, U.S.A. Estuar Coast Mar Sci [Internet]. 1977;5:485–96. Available from: http://www.sciencedirect.com/science/article/pii/0302352477900962

26. Allen GP, Salomon JC, Bassoullet P, Du Penhoat Y, de Grandpré C. Effects of tides on mixing and suspended sediment transport in macrotidal estuaries. Sediment Geol [Internet]. Elsevier; 1980 [cited 2019 Feb 13];26:69–90. Available from: https://www.sciencedirect.com/science/article/pii/0037073880900068

27. Garvine RW. A simple model of estuarine subtidal fluctuations forced by local and remote wind stress. J Geophys Res [Internet]. John Wiley & Sons, Ltd; 1985 [cited 2019 Feb 13];90:11945–8. Available from: http://doi.wiley.com/10.1029/JC090iC06p11945

28. Simpson JH, Brown J, Matthews J, Allen G. Tidal straining, density currents, and stirring in the control of estuarine stratification. Estuaries [Internet]. 1990;13:125–32. Available from: https://doi.org/10.2307/1351581

29. Maie N, Boyer JN, Yang C, Jaffé R. Spatial, geomorphological, and seasonal variability of CDOM in estuaries of the Florida Coastal Everglades. Hydrobiologia [Internet]. 2006;569:135–50. Available from: https://doi.org/10.1007/s10750-006-0128-x

30. Badr E-SA, Tappin AD, Achterberg EP. Distributions and seasonal variability of dissolved organic nitrogen in two estuaries in SW England. Mar Chem [Internet]. 2008;110:153–64. Available from: http://www.sciencedirect.com/science/article/pii/S0304420308000686

31. Muylaert K, Sabbe K, Vyverman W. Spatial and Temporal Dynamics of Phytoplankton Communities in a Freshwater Tidal Estuary (Schelde, Belgium). Estuar Coast Shelf Sci [Internet]. 2000;50:673–87. Available from: http://www.sciencedirect.com/science/article/pii/S0272771400905900

32. Bernhard AE, Colbert D, McManus J, Field KG. Microbial community dynamics based on 16S rRNA gene profiles in a Pacific Northwest estuary and its tributaries. FEMS Microbiol Ecol [Internet]. 2005;52:115–28. Available from: http://dx.doi.org/10.1016/j.femsec.2004.10.016

33. Henriques IS, Alves A, Tacão M, Almeida A, Cunha Â, Correia A. Seasonal and spatial variability of free-living bacterial community composition along an estuarine gradient (Ria de Aveiro, Portugal). Estuar Coast Shelf Sci [Internet]. 2006;68:139–48. Available from: http://www.sciencedirect.com/science/article/pii/S0272771406000497

34. Lv X, Ma B, Yu J, Chang SX, Xu J, Li Y, et al. Bacterial community structure and function shift along a successional series of tidal flats in the Yellow River Delta. Sci Rep [Internet]. 2016;6:36550. Available from: http://dx.doi.org/10.1038/srep36550

35. Aguirre M, Abad D, Albaina A, Cralle L, Goñi-Urriza MS, Estonba A, et al. Unraveling the environmental and anthropogenic drivers of bacterial community changes in the Estuary of Bilbao and its tributaries. Kelly JJ, editor. PLoS One [Internet]. Public Library of Science; 2017 [cited 2019 Jul 12];12:e0178755. Available from: http://dx.plos.org/10.1371/journal.pone.0178755

36. Zaikova E, Walsh DA, Stilwell CP, Mohn WW, Tortell PD, Hallam SJ. Microbial community dynamics in a seasonally anoxic fjord: Saanich Inlet, British Columbia. Environ Microbiol [Internet]. John Wiley & Sons, Ltd (10.1111); 2010 [cited 2019 Feb 13];12:172–91. Available from: http://doi.wiley.com/10.1111/j.1462-2920.2009.02058.x

37. Oren A. Characterization of Pigments of Prokaryotes and Their Use in Taxonomy and Classification. Methods Microbiol [Internet]. Academic Press; 2011 [cited 2019 Mar 26];38:261–82. Available from: https://www.sciencedirect.com/science/article/pii/B9780123877307000127

38. Srinivas TNR, Anil Kumar P, Sucharitha K, Sasikala C, Ramana C V. Allochromatium phaeobacterium sp. nov. Int J Syst Evol Microbiol. 2009;59:750–3.

39. Caumette P, Imhoff JF, Süling J, Matheron R. Chromatium glycolicum sp. nov., a moderately halophilic purple sulfur bacterium that uses glycolate as substrate. Arch Microbiol. 1997;167:11–8.

40. Stomp M, van Dijk MA, van Overzee HMJ, Wortel MT, Sigon CAM, Egas M, et al. The timescale of phenotypic plasticity and its impact on competition in fluctuating environments. Am Nat [Internet]. The University of Chicago Press; 2008 [cited 2019 Mar 26];172:169–85. Available from: https://www.journals.uchicago.edu/doi/10.1086/591680

41. Borrego CM, Gerola PD, Miller M, Cox RP. Light intensity effects on pigment composition and organisation in the green sulfur bacterium Chlorobium tepidum. Photosynth Res [Internet]. Kluwer Academic Publishers; 1999 [cited 2019 Mar 26];59:159–66. Available from: http://link.springer.com/10.1023/A:1006161302838

42. Brown CT, Olm MR, Thomas BC, Banfield JF. Measurement of bacterial replication rates in microbial communities. Nat Biotechnol [Internet]. Nature Publishing Group; 2016 [cited 2018 Dec 18];34:1256–63. Available from: http://www.nature.com/articles/nbt.3704

43. Makarova KS, Wolf YI, Alkhnbashi OS, Costa F, Shah SA, Saunders SJ, et al. An updated evolutionary classification of CRISPR-Cas systems. Nat Rev Microbiol. Nature Publishing Group; 2015;13:722–36.

44. Grissa I, Vergnaud G, Pourcel C. The CRISPRdb database and tools to display CRISPRs and to generate dictionaries of spacers and repeats. BMC Bioinformatics. 2007;8:1–10.

45. Finster K, Bak F, Pfennig N. Desulfuromonas acetexigens sp. nov., a dissimilatory sulfur-reducing eubacterium from anoxic freshwater sediments. Arch Microbiol [Internet]. Springer-Verlag; 1994 [cited 2019 Feb 8];161:328–32. Available from: http://link.springer.com/10.1007/BF00303588

46. Finster K, Coates JD, Liesack W, Pfennig4 N. Desulfuromonas thiophila sp. nov., a New Obligately Sulfur-Reducing Bacterium from Anoxic Freshwater Sediment. Int J Syst Bacteriol. 1997;754–8.

47. Pfennig N, Biebl H. Desulfuromonas acetoxidans gen. nov. and sp. nov., a new anaerobic, sulfur-reducing, acetate-oxidizing bacterium. Arch Microbiol [Internet]. Springer-Verlag; 1976 [cited 2019 Feb 8];110:3–12. Available from: http://link.springer.com/10.1007/BF00416962

48. Tonolla M, Peduzzi S, Demarta A, Peduzzi R, Hahn D. Phototropic sulfur and sulfate-reducing bacteria in the chemocline of meromictic Lake Cadagno, Switzerland. J Limnol [Internet]. 2004 [cited 2019 Jul 9];63:161. Available from: http://jlimnol.it/index.php/jlimnol/article/view/jlimnol.2004.161

49. Wanner G, Vogl K, Overmann J. Ultrastructural characterization of the prokaryotic symbiosis in "Chlorochromatium aggregatum". J Bacteriol [Internet]. American Society for Microbiology Journals; 2008 [cited 2019 Apr 8];190:3721–30. Available from: http://www.ncbi.nlm.nih.gov/pubmed/18344357

50. Findlay AJ. Microbial impact on polysulfide dynamics in the environment. Boden R, editor. FEMS Microbiol Lett [Internet]. Narnia; 2016 [cited 2019 Jul 24];363:fnw103. Available from: https://academic.oup.com/femsle/article-lookup/doi/10.1093/femsle/fnw103

51. Welte C, Hafner S, Krätzer C, Quentmeier A, Friedrich CG, Dahl C. Interaction between Sox proteins of two physiologically distinct bacteria and a new protein involved in thiosulfate oxidation. FEBS Lett [Internet]. John Wiley & Sons, Ltd; 2009 [cited 2019 Jul 8];583:1281–6. Available from: http://doi.wiley.com/10.1016/j.febslet.2009.03.020

52. Alexander B, Imhoff JF. Communities of green sulfur bacteria in marine and saline habitats analyzed by gene sequences of 16S rRNA and Fenna-Matthews-Olson protein. Int Microbiol. 2006;9:259–66.

53. Veldhuis MJW, Gemerden H. Competition between purple and brown phototrophic bacteria in stratified lakes: sulfide, acetate, and light as limiting factors. FEMS Microbiol Lett [Internet]. Narnia; 1986 [cited 2019 Jul 11];38:31–8. Available from: https://academic.oup.com/femsec/article-lookup/doi/10.1111/j.1574-6968.1986.tb01936.x

54. Tonolla M, Peduzzi R, Hahn D. Long-term population dynamics of phototrophic sulfur bacteria in the chemocline of Lake Cadagno, Switzerland. Appl Environ Microbiol [Internet]. American Society for Microbiology; 2005 [cited 2019 Jul 9];71:3544–50. Available from: http://www.ncbi.nlm.nih.gov/pubmed/16000760

55. Eckert W, Frevert T, Dan TB-B, Cavari BZ. Competitive development of *Thiocapsa roseopersicina* and *Chlorobium phaebacteroides* in Lake Kinneret. Can J Microbiol [Internet]. NRC Research Press Ottawa, Canada ; 1986 [cited 2019 Jul 9];32:917–21. Available from: http://www.nrcresearchpress.com/doi/10.1139/m86-169

56. Findlay AJ, Bennett AJ, Hanson TE, Luther GW. Light-Dependent Sulfide Oxidation in the Anoxic Zone of the Chesapeake Bay Can Be Explained by Small Populations of Phototrophic Bacteria. Appl Environ Microbiol [Internet]. 2015;81:7560–9. Available from: http://aem.asm.org/content/81/21/7560.abstract

57. Herbert RA, Tanner AC. The Isolation and Some Characteristics of Photosynthetic Bacteria (Chromatiaceae and Chlorobiaceae) from Antarctic Marine Sediments. J Appl Bacteriol [Internet]. 1977;43:437–45. Available from: http://dx.doi.org/10.1111/j.1365-2672.1977.tb00770.x

58. Parkin TB, Brock TD. The effects of light quality on the growth of phototrophic bacteria in lakes. Arch Microbiol [Internet]. 1980;125:19–27. Available from: https://doi.org/10.1007/BF00403193

59. Manske AK, Glaeser J, Kuypers MMM, Overmann J. Physiology and Phylogeny of Green Sulfur Bacteria Forming a Monospecific Phototrophic Assemblage at a Depth of 100 Meters in the Black Sea. Appl Environ Microbiol [Internet]. 2005;71:8049–60. Available from: http://aem.asm.org/content/71/12/8049.abstract

60. Máthé I, Borsodi AK, Tóth EM, Felföldi T, Jurecska L, Krett G, et al. Vertical physico-chemical gradients with distinct microbial communities in the hypersaline and heliothermal Lake Ursu (Sovata, Romania). Extremophiles [Internet]. 2014;18:501–14. Available from: https://doi.org/10.1007/s00792-014-0633-1

61. Gregersen LH, Habicht KS, Peduzzi S, Tonolla M, Canfield DE, Miller M, et al. Dominance of a clonal green sulfur bacterial population in a stratified lake. FEMS Microbiol Ecol [Internet]. 2009;70:30–41. Available from: http://dx.doi.org/10.1111/j.1574-6941.2009.00737.x

62. Armitage DW, Gallagher KL, Youngblut ND, Buckley DH, Zinder SH. Millimeter-scale patterns of phylogenetic and trait diversity in a salt marsh microbial mat. Front Microbiol [Internet]. Frontiers; 2012 [cited 2019 Mar 20];3:293. Available from: http://journal.frontiersin.org/article/10.3389/fmicb.2012.00293/abstract

63. Pierson B, Oesterle A, Murphy GL. Pigments, light penetration, and photosynthetic activity in the multi-layered microbial mats of Great Sippewissett Salt Marsh, Massachusetts. FEMS Microbiol Lett. 1987;45:365–76.

64. Nicholson JAM, Stolz JF, Pierson BK. Structure of a microbiol mat at Great Sippewissett Marsh, Cape Cod, Massachusetts. FEMS Microbiol Lett. 1987;45:343–64.

65. Bolhuis H, Cretoiu MS, Stal LJ. Molecular ecology of microbial mats. FEMS Microbiol Ecol

[Internet]. Oxford University Press; 2014 [cited 2019 Mar 20];90:335–50. Available from: https://academic.oup.com/femsec/article/90/2/335/2680422/Molecular-ecology-of-microbial-mats

66. Bolhuis H, Stal LJ. Analysis of bacterial and archaeal diversity in coastal microbial mats using massive parallel 16S rRNA gene tag sequencing. ISME J [Internet]. International Society for Microbial Ecology; 2011;5:1701–12. Available from: http://dx.doi.org/10.1038/ismej.2011.52

67. Hamilton TL, Bovee RJ, Thiel V, Sattin SR, Mohr W, Schaperdoth I, et al. Coupled reductive and oxidative sulfur cycling in the phototrophic plate of a meromictic lake. Geobiology [Internet]. John Wiley & Sons, Ltd (10.1111); 2014 [cited 2019 Jul 9];12:451–68. Available from: http://doi.wiley.com/10.1111/gbi.12092

68. Ogawa T, Furusawa T, Nomura R, Seo D, Hosoya-Matsuda N, Sakurai H, et al. SoxAX binding protein, a novel component of the thiosulfate-oxidizing multienzyme system in the green sulfur bacterium Chlorobium tepidum. J Bacteriol [Internet]. American Society for Microbiology Journals; 2008 [cited 2019 Jul 10];190:6097–110. Available from: http://www.ncbi.nlm.nih.gov/pubmed/18641134

69. Cotter PA, Chepuri V, Gennis RB, Gunsalus RP. Cytochrome o (cyoABCDE) and d (cydAB) oxidase gene expression in Escherichia coli is regulated by oxygen, pH, and the fnr gene product. J Bacteriol [Internet]. American Society for Microbiology Journals; 1990 [cited 2019 Jul 10];172:6333–8. Available from: http://www.ncbi.nlm.nih.gov/pubmed/2172211

70. Llorens-Marès T, Liu Z, Allen LZ, Rusch DB, Craig MT, Dupont CL, et al. Speciation and ecological success in dimly lit waters: Horizontal gene transfer in a green sulfur bacteria bloom unveiled by metagenomic assembly. ISME J. 2017;11:201–11.

71. Borton MA, Daly RA, O'Banion B, Hoyt DW, Marcus DN, Welch S, et al. Comparative genomics and physiology of the genus *Methanohalophilus* , a prevalent methanogen in hydraulically fractured shale. Environ Microbiol. 2018;20:4596–611.

72. Daly RA, Roux S, Borton MA, Morgan DM, Johnston MD, Booker AE, et al. Viruses control dominant bacteria colonizing the terrestrial deep biosphere after hydraulic fracturing. Nat Microbiol. 2019;4:352–61.

73. Daly RA, Borton MA, Wilkins MJ, Hoyt DW, Kountz DJ, Wolfe RA, et al. Microbial metabolisms in a 2.5-km-deep ecosystem created by hydraulic fracturing in shales. Nat Microbiol [Internet]. Macmillan Publishers Limited; 2016;1:16146. Available from: http://dx.doi.org/10.1038/nmicrobiol.2016.146

74. Goodcare N, Aljanahi A, Nandakumar S, Mikailov M, Khan AS. A Reference Viral Database (RVDB) To Enhance Bioinformatics Analysis of High-Throughput Sequencing for Novel Virus Detection. mSphere. 2018;3:1–18.

75. Stookey LL. Ferrozine---a new spectrophotometric reagent for iron. Anal Chem [Internet]. American Chemical Society; 1970 [cited 2019 Feb 13];42:779–81. Available from: http://pubs.acs.org/doi/abs/10.1021/ac60289a016

76. Cline JD. Spectrophotometric determination of hydrogen sulfide in natural waters. Limnol

904 Oceanogr. 1969;14:454–8.

905 77. Morrison HG, Grim SL, Vineis JH, Mitchell LS. 16S amplicon fusion primers and protocol
906 for Illumina platform sequencing [Internet]. 2013. Available from:
907 https://figshare.com/articles/16S_amplicon_fusion_primers_and_protocol_for_Illumina_platfor
908 m_sequencing/833944

909 78. Schloss PD, Westcott SL, Ryabin T, Hall JR, Hartmann M, Hollister EB, et al. Introducing
910 mothur: Open-source, platform-independent, community-supported software for describing and
911 comparing microbial communities. Appl Environ Microbiol. 2009;75:7537–41.

912 79. Martin M. Cutadapt removes adapter sequences from high-throughput sequencing reads.
913 EMBnet.journal [Internet]. 2011 [cited 2019 Feb 25];17:10. Available from:
914 http://journal.embnet.org/index.php/embnetjournal/article/view/200

915 80. Callahan BJ, McMurdie PJ, Rosen MJ, Han AW, Johnson AJA, Holmes SP. DADA2: High-
916 resolution sample inference from Illumina amplicon data. Nat Methods [Internet]. Nature
917 Publishing Group, a division of Macmillan Publishers Limited. All Rights Reserved.;
918 2016;13:581–3. Available from: http://dx.doi.org/10.1038/nmeth.3869

919 81. Quast C, Pruesse E, Yilmaz P, Gerken J, Schweer T, Yarza P, et al. The SILVA ribosomal
920 RNA gene database project: improved data processing and web-based tools. Nucleic Acids Res
921 [Internet]. 2013;41:D590–6. Available from:
922 http://nar.oxfordjournals.org/content/41/D1/D590.abstract

923 82. Wickham H. stringr: Simple, Consistent Wrappers for Common String Operations. 2018.

924 83. Wickham H. ggplot2: Elegant Graphics for Data Analysis. [Internet]. New York: Springer-
925 Verlag New York; 2009. Available from: http://ggplot2.org

926 84. Oksanen J, Blanchet FG, Kindt R, Legendre P, Minchin PR, O´Hara RB, et al. vegan:
927 Community Ecology Package. 2012; Available from: http://cran.r-project.org/package=vegan

928 85. Roberts DW. labdsv: Ordination and Multivariate Analysis for Ecology [Internet]. 2012.
929 Available from: http://cran.r-project.org/package=labdsv

930 86. Conway JR, Lex A, Gehlenborg N. UpSetR: An R Package For The Visualization Of
931 Intersecting Sets And Their Properties. bioRxiv [Internet]. 2017; Available from:
932 http://biorxiv.org/content/early/2017/03/25/120600.abstract

933 87. Wickham H, François R, Henry L, Müller K. dplyr: A Grammar of Data Manipulation. 2018.

934 88. Hill TCJ, Walsh KA, Harris JA, Moffett BF. Using ecological diversity measures with
935 bacterial communities. 2003;43:1–11.

936 89. Schmieder R, Edwards R. Quality control and preprocessing of metagenomic datasets.
937 Bioinformatics [Internet]. Oxford University Press; 2011 [cited 2019 Feb 4];27:863–4. Available
938 from: http://www.ncbi.nlm.nih.gov/pubmed/21278185

939 90. Bankevich A, Nurk S, Antipov D, Gurevich A a., Dvorkin M, Kulikov AS, et al. SPAdes: A
940 New Genome Assembly Algorithm and Its Applications to Single-Cell Sequencing. J Comput
941 Biol. 2012;19:455–77.

942 91. Kang DD, Froula J, Egan R, Wang Z. MetaBAT, an efficient tool for accurately
943 reconstructing single genomes from complex microbial communities. PeerJ [Internet]. PeerJ Inc.;
944 2015 [cited 2019 Feb 14];3:e1165. Available from: https://peerj.com/articles/1165

945 92. Eren AM, Esen ÖC, Quince C, Vineis JH, Morrison HG, Sogin ML, et al. Anvi'o: an
946 advanced analysis and visualization platform for 'omics data. PeerJ [Internet]. PeerJ Inc.; 2015
947 [cited 2019 Feb 14];3:e1319. Available from: https://peerj.com/articles/1319

948 93. Parks DH, Imelfort M, Skennerton CT, Hugenholtz P, Tyson GW. CheckM: assessing the
949 quality of microbial genomes recovered from isolates, single cells, and metagenomes. Genome
950 Res [Internet]. 2015;25:1043–55. Available from:
951 http://genome.cshlp.org/content/25/7/1043.abstract

952 94. Silva GGZ, Cuevas D a, Dutilh BE, Edwards R a. FOCUS: an alignment-free model to
953 identify organisms in metagenomes using non-negative least squares. PeerJ. 2014;2:e425.

954 95. Wattam AR, Davis JJ, Assaf R, Boisvert S, Brettin T, Bun C, et al. Improvements to
955 PATRIC, the all-bacterial bioinformatics database and analysis resource center. Nucleic Acids
956 Res. 2017;45:D535–42.

957 96. Couvin D, Bernheim A, Toffano-Nioche C, Touchon M, Michalik J, Néron B, et al.
958 CRISPRCasFinder, an update of CRISRFinder, includes a portable version, enhanced
959 performance and integrates search for Cas proteins. Nucleic Acids Res [Internet]. Oxford
960 University Press; 2018 [cited 2019 Feb 14];46:W246–51. Available from:
961 https://academic.oup.com/nar/article/46/W1/W246/5001162

962 97. Zhang Q, Ye Y. Not all predicted CRISPR–Cas systems are equal: isolated cas genes and
963 classes of CRISPR like elements. BMC Bioinformatics [Internet]. BioMed Central; 2017 [cited
964 2019 Feb 14];18:92. Available from: http://www.ncbi.nlm.nih.gov/pubmed/28166719

965 98. Langmead B, Salzberg SL. Fast gapped-read alignment with Bowtie 2. Nat Methods
966 [Internet]. Nature Publishing Group, a division of Macmillan Publishers Limited. All Rights
967 Reserved.; 2012;9:357. Available from: http://dx.doi.org/10.1038/nmeth.1923

968 99. Meyer F, Paarmann D, D'Souza M, Olson R, Glass EM, Kubal M, et al. The metagenomics
969 RAST server – a public resource for the automatic phylogenetic and functional analysis of
970 metagenomes. BMC Bioinformatics [Internet]. 2008;9:1–8. Available from:
971 http://dx.doi.org/10.1186/1471-2105-9-386

972

973